Non-intrusive POD-based Simulation for Heat Diffusion Systems

G.H. Zhang, *M.Y. Xiao, Y.F. Nie

Department of Applied Mathematics, Northwestern Polytechnical University, Xi'an Shaanxi, P.R. China

*Presenting/Corresponding author: manyuxiao@nwpu.edu.cn

Abstract

Reduced order model constitutes an efficient option to decrease the high computational cost of dynamical systems governed by partial differential equations (PDE). The technique based on proper orthogonal decomposition (POD) was first presented in the article [1] to generate a reduced set of basis functions for Galerkin representation of PDEs which results in approximate the simulation at any time point by solving an ODEs of time dependent coefficients. Our approach in this article targets the development of a non-intrusive reduction technique. We keep the same manner of obtaining basis functions, while approximating the time dependent coefficients using Kriging based surrogate model. The proposed method is then illustrated with an application to the simulations of heat diffusion systems on a thin rod and on a square plate. The numerical results illustrate the simulation using the proposed idea.

Keywords: Proper Orthogonal Decomposition, Kriging surrogate model, heat diffusion system.

1 Introduction

Most of engineering problems may be presented as systems governed by partial differential equations. With the development of science, more rigorous device requirements arise to capture the characteristics of more complex systems, which are common for example in semiconductor manufacturing. The purpose, however, is not to provide an introduction to the complexity of such systems, Instead, we wish to propose a general methodology for implementation of one or two techniques based on surrogate models and apply them to a linear system of heat diffuse equation.

A widely used approach is performing a set of computer experiments 'a priori'. The data sampling is then used for construction of meta-models linking design variables with responses. The literature shows that a wide range of approximation methods that has been used for this purpose, such as polynomial response surfaces [3], least squares approximation [4], Kriging [5], radial basis functions [6] etc. In particular, surrogate model, developed by Krige [7] and then improved by Matheron [8], is emphasized here, as it is an exact interpolation method and a form of generalized linear regression for the formulation of an optimal estimator in a minimum mean square error sense. Due to the superiority of Kriging, it is widely used in structural reliability [9] and in optimization analysis [10].

Another class of among so-called physical based models, the popular one is Proper Orthogonal Decomposition (POD) also known as Karhunen-Loeve expansions in signal analysis and pattern recognition [11], or the Principal Component Analysis in statistics [12], or the method of empirical orthogonal functions in geophysical fluid dynamics [13,14]. Detailed description of the POD can be found in [15]. POD provides a useful tool for efficiently approximating a large amount of data. Lumley [16] first used POD to study turbulent flows. In 1987, Sirovich [17] incorporated the method of 'snapshots' into the POD framework and made important progress in this field. Other applications of POD are given in [18-20].

In this paper, a technique combining the advantages of Kriging surrogate model and POD model is proposed to represent heat diffusion on a one- or two- dimensional spatial domain. Suppose a given set of data sampling, discretization of PDE is approximately executed with the Galerkin method.

Then, we construct a basis of the finite dimensional function space of interest. In [2], the time dependent coefficients are obtained by solving an ODE. Here we propose a "non-intrusive" technique. Based on the original discrete data information, the approximated representation is built with Kriging surrogate model for the POD coefficients. It is finally applied to obtain the temperature field for any untried time point.

The paper is organized as follows: In section 2 we present the simulation of heat diffusion on a thin rod (one-dimensional spatial domain) and on a square plate (two-dimensional spatial domain) using infinite series expansion and finite difference scheme. Then we review the Galerkin projection and the POD model in the section 3. In section 4, a new method combining POD and Kriging surrogate model is described, and illustrates feasibility and efficiency of the proposed technique, followed by the numerical results in Section 5. The paper ends with conclusions and prospects.

2 Description of Heat Diffusion Equation

We consider an initial boundary value problem (IBVP) of heat equation. The methodology of "high fidelity" simulation is then explained to get the sampling data.
Case1: the one-dimension (1D) simulation of heat diffusion equation:

$$\begin{array}{lll} \text{PDE} & \boldsymbol{u}_t = \boldsymbol{u}_{xx} & x \in (0,1); \quad t > 0 \\ \text{BCs} & \boldsymbol{u}(0,t) = 0 = \boldsymbol{u}(1,t) & t > 0 \\ \text{IC} & \boldsymbol{u}(x,0) = 1 & x \in (0,1) \end{array} \tag{1}$$

where $\boldsymbol{u}(x,t)$ represents the temperature field on a thin rod.
Similarly, the case 2 is given by the following IBVP with two-dimension (2D) simulations:

$$\begin{array}{lll} \text{PDE} & \boldsymbol{u}_t = \boldsymbol{u}_{xx} + \boldsymbol{u}_{yy} & x \in (0,1); \quad y \in (0,1); \quad t > 0 \\ \text{BCs} & \boldsymbol{u}(0,y,t) = 0 = \boldsymbol{u}(1,y,t) & t > 0 \\ & \boldsymbol{u}(x,0,t) = 0 = \boldsymbol{u}(x,1,t) & t > 0 \\ \text{IC} & \boldsymbol{u}(x,y,0) = 1 & x \in (0,1); \quad y \in (0,1) \end{array} \tag{2}$$

where $\boldsymbol{u}(x,y,t)$ represents the temperature field on a flat plate.

2.1 Methodology

In order to obtain a set of "high fidelity" simulation data. A convenient method is to evaluate the infinite series solutions to the respective IBVPs at a set of spatial points and temporal values.
The infinite series solution to IBVP (1) is given by

$$\boldsymbol{u}(\boldsymbol{x},t) = \sum_{n=1}^{\infty} \boldsymbol{A}_n e^{-n^2\pi^2 t} \sin(n\pi \boldsymbol{x}) \tag{3}$$

where $\boldsymbol{A}_n = \frac{2}{n\pi}(1-\cos(n\pi))$. And the infinite solution to IBVP (2) is given by

$$\boldsymbol{u}(\boldsymbol{x},\boldsymbol{y},t) = \sum_{m,n=1}^{\infty} \boldsymbol{A}_{mn} e^{-(m^2+n^2)\pi^2 t} \sin(m\pi \boldsymbol{x}) \sin(n\pi \boldsymbol{y}) \tag{4}$$

where $A_{mn} = \frac{4}{mn\pi^2}(1-\cos(m\pi))(1-\cos(n\pi))$.

An alternative method is to solve this equation numerically. We approximate all the derivatives by finite differences with a second-order central difference scheme for the spatial derivative at position and the forward difference in time. The discrete form is then written as:

1D:

$$\frac{u_i^{n+1}-u_i^n}{\Delta t} = \frac{u_{i+1}^n - 2u_i^n + u_{i-1}^n}{\Delta x^2} \tag{5}$$

2D:

$$\frac{u_{i,j}^{n+1}-u_{i,j}^n}{\Delta t} = \frac{u_{i+1,j}^n - 2u_{i,j}^n + u_{i-1,j}^n}{\Delta x^2} + \frac{u_{i,j+1}^n - 2u_{i,j}^n + u_{i,j-1}^n}{\Delta y^2} \tag{6}$$

where Δt is time step, Δx and Δy are space steps in direction x and y respectively, $n = 0,1,2,\cdots$; $i = 0,1,\cdots I$; $j = 0,1,\cdots,J$.

So, with these recurrence relations, and knowing the values at time n, one can obtain the corresponding values at time $n+1$. $u_0^n, u_{0,0}^n$ and $u_I^n, u_{I,J}^n$ must be replaced by the boundary conditions. Furthermore, based on the initial conditions, $u_i^0, u_{i,j}^0$ are all given.

2.2 "High fidelity" simulation analysis

The aim in this section is to compare the difference of two "high fidelity" simulations. More precisely, above two methodologies are used to simulate the temperature field at each value of time in the set for IBVP (1) {0.00, 0.001, 0.002, …, 0.200} and in IBVP (2) in the set {0.00, 0.05, 0.10, …, 0.45, 0.50}. The space step is 0.01 in 1D and 0.01×0.01 in 2D. Several temperature distributions are shown in Figure 1. The data was stored for use as empirical data in the POD.

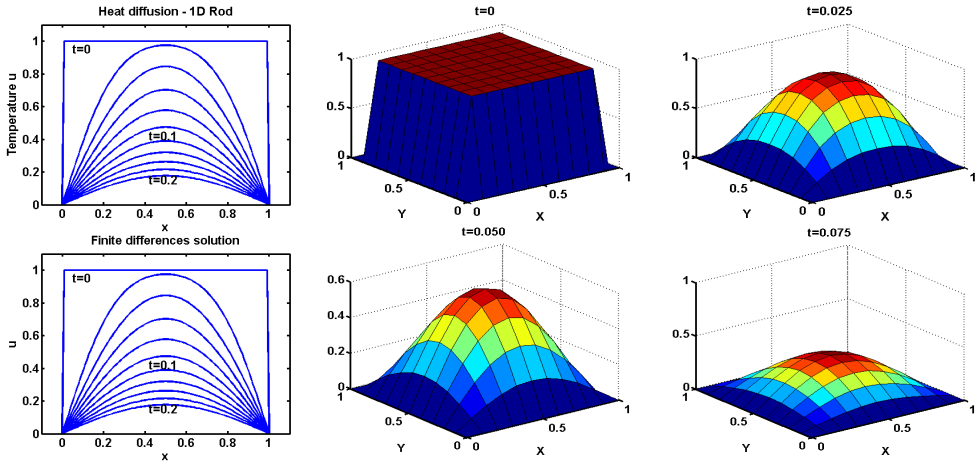

Figure 1. Top Left: Simulation of IBVP (1): time dependent heat diffusion on 1D rod with constant initial condition and zero boundary conditions. Bottom Left: The finite differences simulation of IBVP (1). Right: Simulation of IBVP (2): time dependent heat diffusion on 2D plate with constant initial condition and zero boundary conditions.

From Figure 1, we can observe that the simulations using analytical functions coincide with those obtained by the numerical method.

3 Approximate simulation based on the Galerkin Method and the POD

This section includes a brief overview of the Galerkin method for PDE discretization and implementation of POD to get an orthogonal basis of space domain.

3.1 Discretization with the Galerkin method

The Galerkin method is a discretization scheme for PDEs which is one type of spectral methods or methods of weighted residuals. The main idea is to separate variables and to represent a field with a truncated series expansion given by

$$\boldsymbol{u}(\boldsymbol{x},t)=\sum_{i=1}^{N}\alpha_i(t)\boldsymbol{\varphi}_i(\boldsymbol{x}) \tag{7}$$

where $\boldsymbol{\varphi}_i(\boldsymbol{x})$ are trial functions which can form an orthonormal basis for the approximate function space. $\alpha_i(t)$ are time dependent coefficients obtained by minimizing the residuals or errors between approximate and exact values. Equivalently, the residuals must be orthogonal to each one of the given trial functions. Thus, the original infinite dimensional system can be approximated by an *N*-dimensional one.

3.2 Construction of reduced basis function via the POD

As stated earlier, a set of "high fidelity" simulations is recorded yielding the snapshots of the heat equation solution for IBVP (1) at *M*=200 equally spaced sample times between $t=0$ and $t=0.200$, and at *M*=20 equally spaced sample times between $t=0$ and $t=0.5$ for IBVP (2) (the IC was also used as the first snapshot). These snapshots are used as the empirical data for computing a set of basis functions via the POD.

If we denote the set of original snapshots as $\{\boldsymbol{u}(\boldsymbol{x},t_k):k=1,2,...,M\}$ then the average snapshot is computed as

$$\bar{\boldsymbol{u}}(\boldsymbol{x})=\frac{1}{M}\sum_{k=1}^{M}\boldsymbol{u}(\boldsymbol{x},t_k) \tag{8}$$

and the centered snapshots are given by

$$\boldsymbol{v}^{(k)}=\boldsymbol{v}(\boldsymbol{x},\boldsymbol{t}_k)=\boldsymbol{u}(\boldsymbol{x},\boldsymbol{t}_k)-\bar{\boldsymbol{u}}(\boldsymbol{x}) \tag{9}$$

This adjustment leaves us with a new ensemble of data samples $\{\boldsymbol{v}(\boldsymbol{x},t_k):k=1,....M\}$. These snapshots are then used to compute the $M\times M$ empirical correlation matrix $\boldsymbol{C}$ whose entries are given by

$$(\boldsymbol{C})_{ij}=\frac{1}{M}\int_{\Omega}v^{(i)}(x)v^{(j)}(x)dx \quad i,j=1,\cdots,M \tag{10}$$

where Ω is the spatial domain ([0,1]). The problem is reduced to finding the eigenvectors and eigenvalues of $\boldsymbol{C}$, and the eigenvectors $\boldsymbol{A}^{(n)}$ of $\boldsymbol{C}$ and the corresponding eigenvalues λ_n satisfy

$$\boldsymbol{C}\boldsymbol{A}^{(n)}=\lambda_n\boldsymbol{A}^{(n)} \quad n=1,...,M \tag{11}$$

which can be solved for corresponding system of M eigenvalues and M eigenvectors. The numerical integration (10) is hard-coded using a simple approximation technique. The eigenvalues and eigenvectors of $\boldsymbol{C}$ are then used to compute the empirically determined eigenfunctions, and the basis functions are then computed as linear combinations of data samples using

$$\boldsymbol{\varphi}_n(\boldsymbol{x}) = \sum_{k=1}^{M} \boldsymbol{A}_k^{(n)} \boldsymbol{v}^{(k)}(\boldsymbol{x}) \quad n = 1,\ldots,M \tag{12}$$

It is easy to check

$$(\boldsymbol{\varphi}_l, \boldsymbol{\varphi}_m) = \begin{cases} 1 & l = m \\ 0 & l \neq m \end{cases}. \tag{13}$$

This completes the construction of the orthonormal set $\{\boldsymbol{\varphi}_1, \boldsymbol{\varphi}_2, \ldots, \boldsymbol{\varphi}_M\}$.
By utilizing the properties of the POD one can specify an energy level e to be captured and then seek $N<<M$ such that

$$\frac{\sum_{i=1}^{N} \lambda_i}{\sum_{i=1}^{M} \lambda_i} > e .$$

Then, based on the Galerkin method, the approximation $\hat{\boldsymbol{v}}$ to the $\boldsymbol{v}(\boldsymbol{x},t)$ is given by the truncated series expansion

$$\hat{\boldsymbol{v}}(\boldsymbol{x},t) = \sum_{n=1}^{N} \alpha_n(t) \boldsymbol{\varphi}_n(\boldsymbol{x}). \tag{14}$$

The average snapshot $\bar{\boldsymbol{u}}$ is then added

$$\hat{\boldsymbol{u}}(\boldsymbol{x},t) = \bar{\boldsymbol{u}}(\boldsymbol{x}) + \hat{\boldsymbol{v}}(\boldsymbol{x},t) \tag{15}$$

to reconstruct the original data samples. The approximation order N can be varied to achieve the desired degree of accuracy.
The $\alpha_n(t)$ are time-dependent coefficients chosen to ensure the original PDE satisfied as closely as possible by (14). This is achieved by minimizing the residual. More details are discussed in the following section.

3.3 Calculation of the coefficients by solving an ODE

We suppose we have a system governed by the PDEs (in symbolic form)

$$\frac{\partial \boldsymbol{v}}{\partial t} = D(\boldsymbol{v}); \quad \boldsymbol{v} : D \times (0,\infty) \to \Re \tag{16}$$

with appropriate boundary conditions and initial conditions, where $D(\square)$ is a spatial operator , e.g. the Laplacian in the case of heat diffusion. Define the residual as

$$\boldsymbol{r}(\boldsymbol{x},t) = \frac{\partial \hat{\boldsymbol{v}}}{\partial t} - D(\hat{\boldsymbol{v}}) . \tag{17}$$

We force the residual to be orthogonal to a suitable number of eigenfunctions, i.e.

$$\left\langle \boldsymbol{r}(\boldsymbol{x},t), \boldsymbol{\varphi}_n(\boldsymbol{x}) \right\rangle = 0 \quad n = 1,\ldots,N . \tag{18}$$

Substituting (14) into (17) yields,

$$\boldsymbol{r}(\boldsymbol{x},t) = \sum_{n=1}^{N} \dot{\alpha}_n(t)\boldsymbol{\varphi}_n(\boldsymbol{x}) - D(\sum_{m=1}^{N} \alpha_m(t)\boldsymbol{\varphi}_m(\boldsymbol{x})) . \tag{19}$$

Applying the orthogonality condition (18) and using the orthonormality property of the set of eigenfunctions results in

$$\dot{\alpha}_i(t) = \int_D D(\sum_{m=1}^{N} \alpha_m(t)\boldsymbol{\varphi}_m(\boldsymbol{x}))\boldsymbol{\varphi}_i(\boldsymbol{x})d\boldsymbol{x} \quad i = 1,\ldots,N \tag{20}$$

Thus, requiring the residual be orthogonal to the first N eigenfunctions yields a system of N ordinary differential equations in t (an N^{th} -order system)

$$\dot{\boldsymbol{\alpha}} = F(\boldsymbol{\alpha}) \tag{21}$$

where $\boldsymbol{\alpha} = (\alpha_1,\ldots,\alpha_N)$ and $F : \Re^N \to \Re^N$.
The initial conditions for the resulting system of ODEs are determined by a second application of the Galerkin approach. We force the residual $\boldsymbol{I}(\boldsymbol{x}) = \boldsymbol{v}(\boldsymbol{x},0) - \hat{\boldsymbol{v}}(\boldsymbol{x},0)$ of the initial conditions to also be orthogonal to the first N eigenfunctions. We obtain a system of N linear equations

$$\alpha_i(0) = \int_D \boldsymbol{v}(\boldsymbol{x},0)\boldsymbol{\varphi}_i(\boldsymbol{x})d\boldsymbol{x} \quad i = 1,\ldots,N . \tag{22}$$

The heat diffusion system dynamics are described by

$$\frac{\partial(\boldsymbol{v} + \overline{\boldsymbol{u}})}{\partial t} = D(\boldsymbol{v}) = \nabla^2(\boldsymbol{v} + \overline{\boldsymbol{u}}) \tag{23}$$

Applying (20) yields the system of linear ODEs

$$\dot{\alpha}_i(t) = \sum_{j=1}^{N} \alpha_j(t) \int_D \boldsymbol{\varphi}_i(\boldsymbol{x})\nabla^2\boldsymbol{\varphi}_j(\boldsymbol{x})d\boldsymbol{x} + \int_D \nabla^2\overline{\boldsymbol{u}}(\boldsymbol{x})\boldsymbol{\varphi}_i(\boldsymbol{x})d\boldsymbol{x} \quad i = 1,\ldots,N \tag{24}$$

with initial conditions

$$\alpha_i(0) = \int_D \boldsymbol{\varphi}_i(\boldsymbol{x})\boldsymbol{v}(0,\boldsymbol{x})d\boldsymbol{x} \quad i = 1,\ldots,N \tag{25}$$

where $D = [0,1]$ for the rod. This results in linear system of ODEs

$$\dot{\boldsymbol{\alpha}}(t) = \boldsymbol{\Gamma}\boldsymbol{\alpha}(t) + \boldsymbol{b} \tag{26}$$

where $\boldsymbol{\alpha}(t)$ is an N-vector, $\boldsymbol{\Gamma}$ is the $N \times N$ matrix with entries

$$(\boldsymbol{\Gamma})_{ij} = \int_D \boldsymbol{\varphi}_i(\boldsymbol{x}) \nabla^2 \boldsymbol{\varphi}_j(\boldsymbol{x}) d\boldsymbol{x} \tag{27}$$

and $\boldsymbol{b}$ is an N-vector with elements

$$b_i = \int_D \nabla^2 \overline{u}(\boldsymbol{x}) \boldsymbol{\varphi}_i(\boldsymbol{x}) d\boldsymbol{x} \,. \tag{28}$$

The solution to (26) is given by the variation of constants formula

$$\boldsymbol{\alpha}(t) = e^{\boldsymbol{\Gamma} t}\boldsymbol{\alpha}(0) + \int_0^t e^{\boldsymbol{\Gamma}(t-\tau)} \boldsymbol{b} d\tau \tag{29}$$

where the IC $\boldsymbol{\alpha}(0)$ is an N-vector with entries given by (22). However, rather than hard-code the solution (29) we can numerically integrate (26) using Runge-Kutta method.
Once the ODE (26) is solved and evaluated at the desired values of t, the $\hat{\boldsymbol{u}}(\boldsymbol{x}, t)$ is known.

4 Calculation of the coefficients by Kriging interpolation

Once the set of snapshots $\{\boldsymbol{v}(\boldsymbol{x}, t_k) : k = 1, \ldots, M\}$ and reduced basis functions $\boldsymbol{\varphi}_n$ are obtained, the set of coefficients can be calculated by the projection of those snapshots on the basis fuctions:

$$\alpha_k^{(i)} = < \boldsymbol{v}(\boldsymbol{x}, t_k), \boldsymbol{\varphi}_i >, i = 1, \cdots, M; k = 1, \cdots, M \tag{30}$$

or

$$\alpha_k^{(i)} = < \boldsymbol{u}(\boldsymbol{x}, t_k) - \overline{\boldsymbol{u}}, \boldsymbol{\varphi}_i >, i = 1, \cdots, M; k = 1, \cdots, M \tag{31}$$

where $<\square, \square>$ denotes the inner product.
Then, any general approximation technique may be used to build surrogate response surfaces of each coefficient $\alpha_i(t), i = 1, \cdots, M$. Here, Kriging interpolation is used as it can capture the local phenomena. The simulation of heat diffusion is finally assembled at any time point:

$$\boldsymbol{u\_approx}(\boldsymbol{x}, t) = \overline{\boldsymbol{u}}(\boldsymbol{x}) + \sum_{n=1}^{M} \tilde{\alpha}_n(t) \boldsymbol{\varphi}_n(\boldsymbol{x}) \tag{32}$$

Same as the before, we can using the truncated expansion to evaluate $\boldsymbol{u}(\boldsymbol{x}, t)$ as

$$\boldsymbol{u\_tru}(x, t) = \overline{\boldsymbol{u}}(x) + \sum_{n=1}^{N} \tilde{\alpha}_n(t) \boldsymbol{\varphi}_n(x), \quad N << M \tag{33}$$

4.1 Kriging surrogate model

Kriging meta-model is an interpolation technique based on statistical theory, which consists of a parametric linear regression model and a non-parametric stochastic process. It needs a design of experiments to define its stochastic parameters and then predictions of the response can be completed at any unknown point. Given an initial design of experiments (initial DoE): $\boldsymbol{X} = \{\boldsymbol{x}^{(1)}, \boldsymbol{x}^{(2)}, \ldots, \boldsymbol{x}^{(n)}\}^T$, with observed responses, $\boldsymbol{Y} = \{y^{(1)}, y^{(2)}, \ldots, y^{(n)}\}^T$. $\boldsymbol{Y}$ could be generated by high fidelity simulations or experiments.

Kriging surrogate model presumes the real function relationship between the DoE and the response as

$$y(\boldsymbol{X}) = \mu + Z(\boldsymbol{X}) \tag{34}$$

where μ is a hyperparameter which is determined part and $Z(\boldsymbol{X})$ is a Gaussian stochastic process with zero mean and covariance in the form of

$$\mathrm{Cov}(Z(\boldsymbol{X}^{(i)}), Z(\boldsymbol{X}^{(j)})) = \sigma_z^2 \boldsymbol{R}(\boldsymbol{X}^{(i)}, \boldsymbol{X}^{(j)}) \tag{35}$$

where $\boldsymbol{R}$ is the correlation function between two sample points and σ_z^2 the Gaussian process variance. For $\boldsymbol{R}$, most applications use Gaussian function

$$\boldsymbol{R}(\boldsymbol{X}^{(i)}, \boldsymbol{X}^{(j)}) = \exp(-d(\boldsymbol{X}^{(i)}, \boldsymbol{X}^{(j)})) \tag{36}$$

where $d(\boldsymbol{X}^{(i)}, \boldsymbol{X}^{(j)})$ is the distance function between $\boldsymbol{X}^{(i)}$ and $\boldsymbol{X}^{(j)}$. Usually it is a weighted distance function

$$d(\boldsymbol{X}^{(i)}, \boldsymbol{X}^{(j)}) = \sum_{k=1}^{z} \theta_k \left| x_k^{(i)} - x_k^{(j)} \right|^2 \tag{37}$$

Hyperparameters θ_k control the degree of nonlinearity in kriging surrogate model. Sometimes we choose θ_k equal to 2. Through maximum likelihood prediction, the estimates for μ and σ_z^2 is given

$$\begin{cases} \hat{\mu} = \dfrac{\boldsymbol{I}^{\mathrm{T}} \boldsymbol{\Psi}^{-1} \boldsymbol{Y}}{\boldsymbol{I}^{\mathrm{T}} \boldsymbol{\Psi}^{-1} \boldsymbol{I}} \\ \sigma_z^2 = \dfrac{1}{n} (\boldsymbol{Y} - \boldsymbol{I}\hat{\mu})^{\mathrm{T}} \boldsymbol{\Psi}^{-1} (\boldsymbol{Y} - \boldsymbol{I}\hat{\mu}) \end{cases} \tag{38}$$

where $\boldsymbol{\Psi}$ is a $n \times n$ matrix $(\boldsymbol{\Psi})_{ij} = \boldsymbol{R}(\boldsymbol{X}^{(i)}, \boldsymbol{X}^{(j)})$, $\boldsymbol{I}$ is the unit matrix. Thus the prediction model could be built as

$$y(\boldsymbol{X}) = \hat{\mu} + \boldsymbol{r}^{\mathrm{T}}(\boldsymbol{X}) \boldsymbol{\Psi}^{-1} (\boldsymbol{Y} - \boldsymbol{I}\hat{\mu}) \tag{39}$$

Here $\boldsymbol{r}(\boldsymbol{X}) = [\boldsymbol{R}(\boldsymbol{X}, \boldsymbol{X}^{(1)}), \boldsymbol{R}(\boldsymbol{X}, \boldsymbol{X}^{(2)}), \ldots, \boldsymbol{R}(\boldsymbol{X}, \boldsymbol{X}^{(n)})]^{\mathrm{T}}$.

5 Numerical Analysis

Now, we present some results of the above computations and simulations. The whole process has been performed in four steps:
- A set of basis functions was determined using the POD (according to from Eq.(8) to Eq.(11)) for the 1D heat diffusion system with $M = 201$ snapshots and $M = 21$ in 2D
- Calculation of the coefficients α by projection of snapshots on the basis
- Based on the data obtained in step 1 and 2, the Kriging surrogate model can determine an approximation of coefficients α(t) for any time point
- The simulation is then approximated by Eq. (32) or Eq.(33)

5.1 Eigenvalues and corresponding eigenfunctions

As stated earlier, the eigenvalues measure the relative energy of the system dynamics. Figure 2 shows the resulting empirically determined eigenfunctions for the 1D and 2D heat diffusion systems corresponding to first four eigenvalues in decreasing order.

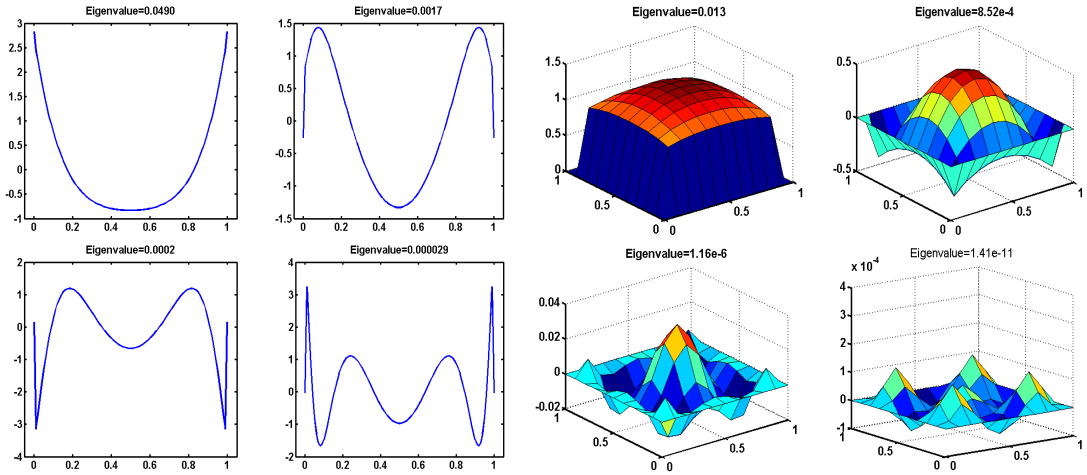

Figure 2. The first four basis functions of the system with corresponding eigenvalues for IBVP (1) (Left) and for IBVP (2)(Right).

From Fig.2, it is readily observed that the four modes contain virtually all of the energy.

5.2 Reconstruction error analysis

The reconstruction errors are calculated for the original snapshots. Figure 3 shows that the relative errors $\|\mathbf{u}-\tilde{\mathbf{u}}\|/\|\mathbf{u}\|$ on the temperature field (Figure 3,left for 1D, right is about 2D) decrease quickly with increasing the number of modes. Furthermore, we observe that the reconstruction errors at the initial time point are slightly smaller than those at other time points. So that'a why in the following Garlerkin approximations, only the first three modes are used (N=3).

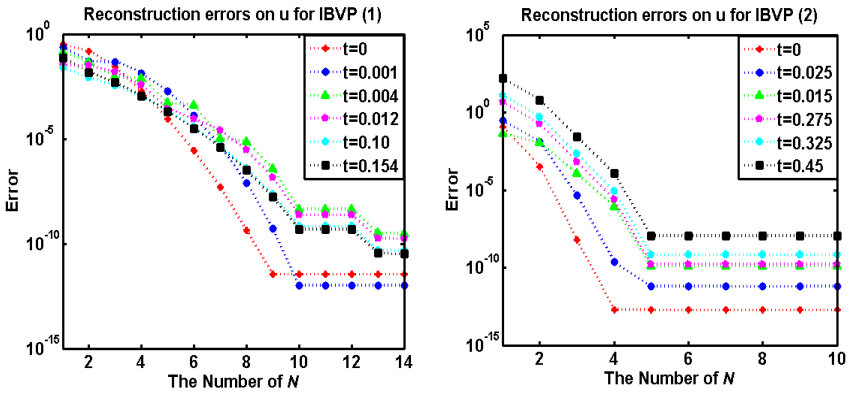

Figure 3. The construction errors on the temperature field u for both two IBVPs.

5.3 Comparison of exact temperature field and its reconstruction

From Figure 4, middle, we observe that the reconstruction temperature field is similar to the exact one. As expected, solution approximated with coefficients based on Kriging interpolation reproduces the original data when the number of POD modes N is chosen to equal the number of snapshots M. While a slight error with the truncation of POD modes, N =3. This can be seen more clearly in Figure 5.

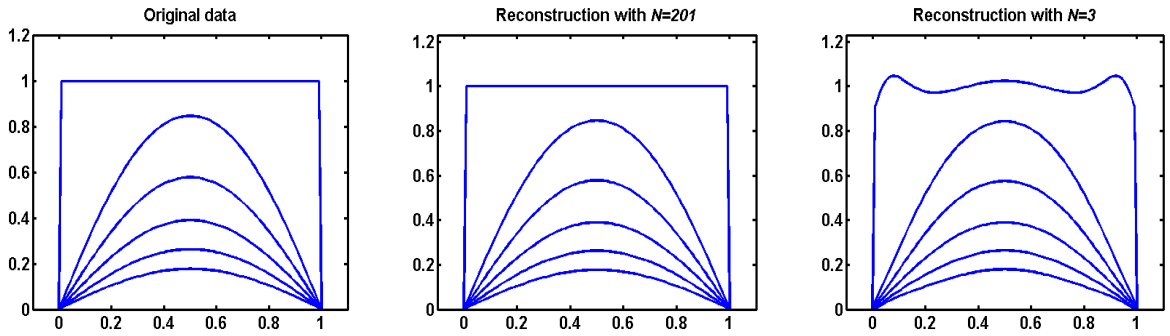

Figure 4. Original heat diffusion data u (top, left) from infinite series solution, and reconstruction temperature field of IBVP(1) using modes N=M=201 or empirical data determined eigenfunctions N(top, right) and ones with N=3 (bottom, left) for $t = 0$, 0.04, 0.08, 0.12, 0.16, 0.20 respectively.

Table 1. The reconstruction error with N=201 and N=3 respectively

Error	t=0.0	t=0.001	t=0.004	t=0.009
$\|u - u\_appox\|/\|u\|$	3.3829e-12	1.0317e-12	1.8553e-12	8.1031e-13
$\|u - u\_tru\|/\|u\|$	0.0270	0.0481	0.0091	0.0156

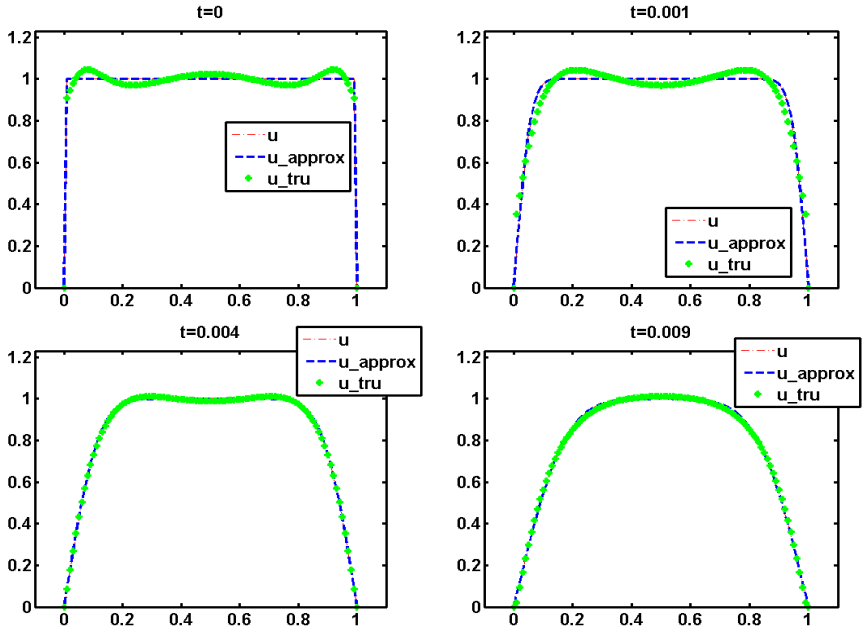

Figure 5. Heat diffusion profiles for $t = 0, 0.001, 0.004, 0.009$**.**

Figure 5 gives to the exact temperature field and reconstruction one at different time points. The errors are given in table 1. We observe that the approximations are accurate. That is to say, the approximation accuracy increases rapidly with time, although there is difficulty in reproducing the initial condition. This phenomenon is due to the fact that the solution progress from a discontinuous initial condition to smooth profiles requires fewer terms to get equivalent accuracy. Similar conclusion is observed for the 2D domain, Figure 6.

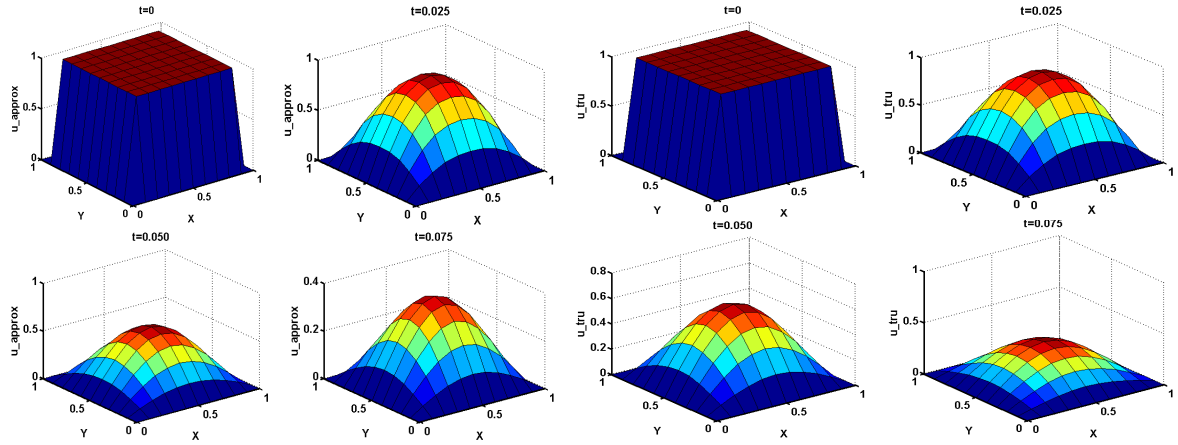

Figure 6. Approximate solutions of IBVP (2) using empirically determined eigenfunctions for *t*=0, 0.025, 0.05, 0.075. Left: 201 eigenfunctions are used. Right: 3 eigenfunctions are used.

As stated earlier, Kriging meta-model is a technique that can provide the predictions of the response at arbitrary point. Therefore, the advantage we used the Kriging to interpolation the coefficient $\boldsymbol{a}(t)$ of POD is that we can calculate the value of $\boldsymbol{u}$ at any time point different from the sampling points. Figure 7 shows the comparison of original data $\boldsymbol{u}$ and others two approximate values with N=201 denoting ***u_approx*** and N=3 for ***u_tru*** at $t = 0.0045, 0.1255, 0.201, 0.210$.

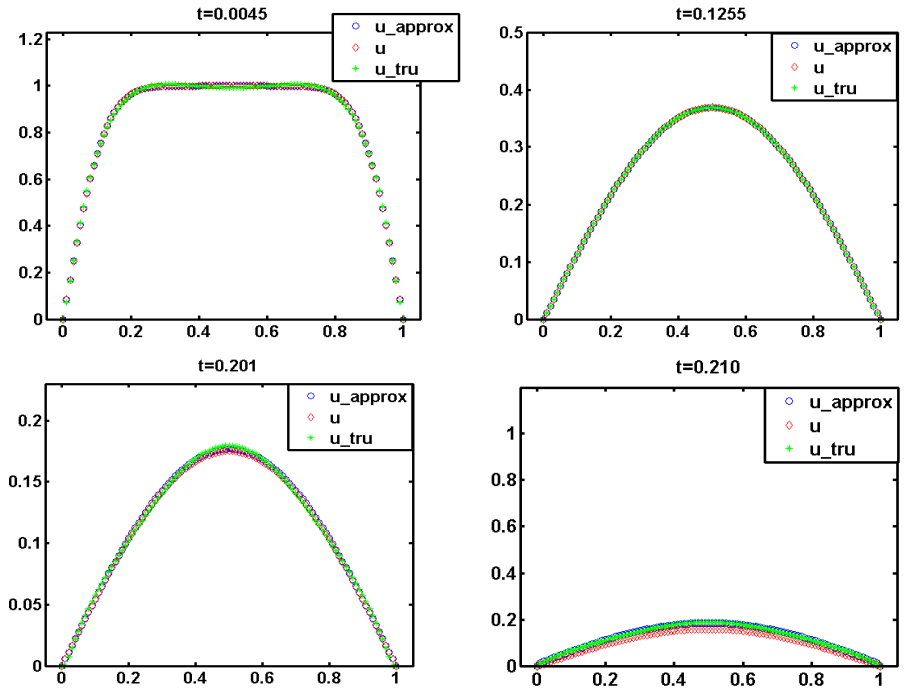

Figure 7. The values of *u*, *u_approx* ,and *u_tru* at $t = 0.0045, 0.1255, 0.201$ and $t = 0.210$.

From Figure 7, we can conclude that the prediction of ***u*** can get good accuracy when the time point t is in the region [0,0.2]. However, when t becomes larger than 0.2, the errors between exact field ***u*** and the approximations ***u_approx*** become much bigger with the time increasing. That is obviously due to the average field computed from the snapshots at the time points belonging in the region [0,0.2].

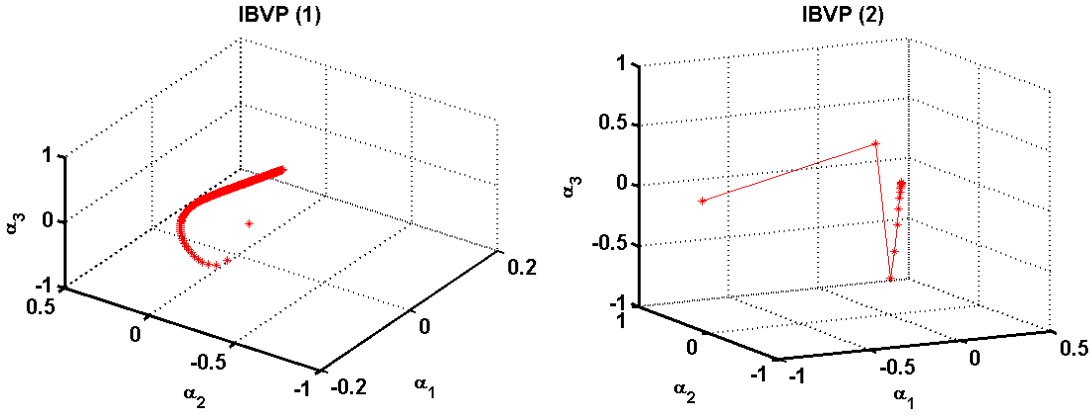

Figure 8. The first three $\alpha_i(t), i = 1,2,3$ for both two heat diffusion equation systems.

In Figure 8 we show the first three $\alpha_i(t)$,i=1,2,3 computed using inner product. It appears better to choose the second order polynomial function for regression in Kriging. While, the linear function for regression in IBVP(2) seeing from the right of Fig.8.

6 Conclusions

In this article, a technique combining the advantages of two types of surrogate models has been proposed to approximate the simulation of PDEs. After descritization of PDEs with the Galerkin method, the basis functions of space are first obtained by the standard POD. The second part consists in approximating the coefficients of Garlerkin discretization form of PDEs using Kriging surrogate model. The resulting reduced order model is then applied to simulate the heat diffusion in one-dimension rod and two-dimension plate. The numerical results show that reconstructed temperature field is efficiently approximated with the non-intrusive POD approach. The reconstruction errors are only controlled by the number of POD basis functions, as the Kriging interpolation of coefficients does not influence the precision of Garlerkin approximation.

In terms of future prospects, we will be interested in using this method to reconstruct the reduced order model for more complex systems and consider the multi-fidelity data at the same time.

7 Acknowledgment

This work has been supported by the National Natural Science Foundation of China (Grants No. 11302173).

References

[1] Andrew J. Newman. (1996) Model reduction via the Karhunen-Loeve expansion part I: An exposition. *Technical report, Institute for Systems Research.*

[2] Andrew J. Newman. (1996) Model reduction via the Karhunen-Loeve expansion part II: Some elementary examples. *Technical report, Institute for Systems Research.*

[3] A. Giunta, L. Watson, J. Koehler. (1998) A Comparison of Approximation Modeling Techniques: Polynomial Versus Interpolating Models. *7th AIAA/USAF/NASA/IS SMO Symposium on Multidisciplinary Analysis & Optimization, Sept 2–4, St. Louis, MI, USA, AIAA*, 1998-4758.

[4] P. Breitkopf, H. Naceur, Rassineux. (2005) A moving least squares response surface approximation: formulation and metal forming applications. *Computers & Structures,* **83**:1411-1428.

[5] S.N. Lophaven, H.B. Nielsen, J. Sondergaard. (2002) DACE-A Matlab Kriging Toolbox. *Informatics and mathematical modeling, Denmark*.

[6] M. Samuelides. (2009) Surfaces de réponse et réduction de modèles, Optimisation multidisciplinaire en mécanique 2, Hermes Science Publications.

[7] M. Guarascio, M. David, C. Hyijbregts. (19750 Advanced geostatistics in mining industry, in: Proceedings of the NATO Advanced Study Institute, *Istituto di Geologia Applicata of the University, Rome, Italy*.

[8] G.Matheron. (1973) The intrinsic random functions and their applications. *Adv. Appl. Probab.* **5**(3): 439-468.

[9] I. Kaymaz. (2005) Application of Kriging method to structural reliability problems. *Struct. Saf.* **27**:133-151.

[10] M. Xiao, P. Breitkopf, R. Filomeno Coelho, C. Knopf-Lenoir, M. Sidorkiewicz, P. Villon. (2010) Model Reduction by CPOD and Kriging - application to the Shape Optimization of an intake port. *Structural and Multidisciplinary Optimization*, **41**(4):555-574.

[11] Holmes P, Lumley J L, Berkooz G. (1996) Turbulence, Coherent Structures, Dynamical Systems and Symmetry. *Cambridge: Cambridge University Press*.

[12] Fukunaga K. (1990) Introduction to Statistical Recognition. *New York: Academic Press*.

[13] Jolliffe I T. (2002) Principal Component Analysis, *Springer-Verlag*.

[14] Crommelin D T, Majda A J. (2004) Strategies for model reduction: comparing different optimal bases. *J Atmospheric Sci,* **61**: 2306-2317.

[15] S.S.Ravindran. (2000) A reduced-order approach for optimal control of fluids using proper orthogonal decomposition, *International Journal For Numerical Methods In Fluids,* **34**: 425-448.

[16] Lumley JL. (1967) The structure of inhomogeneous turbulence. In Atmospheric Turbulence and Radio Wave Propagation, Yaglom AM, Tatarski VA (eds). Nauka: Moscow, 166-178.

[17] Sirovich L. (1987) Tubulence and the dynamics of coherent structures: part I-III. *Quarterly of Applied Mathematics,* **45**(3): 561-590.

[18] Hung V. Ly, Hien T. Tran. (1999) Modeling and control of physical process using proper orthogonal decomposition. *Journal of Mathematical and Computer Modeling*.

[19] M. Xiao, P. Breitkopf, R. Filomeno Coelho, P. Villon, W. Zhang. (2014) Proper orthogonal decomposition with high number of linear constraints for aerodynamical shape optimization, *Applied Mathematics and Computation,* Volume **247**:1096-1112.

[20] M. Xiao, P. Breitkopf, R. Filomeno Coelho, C. Knopf-Lenoir, P. Villon, W. Zhang. (2013) Constrained Proper Orthogonal Decomposition based on QR-factorization for aerodynamical shape optimization. *Applied Mathematics and Computation* **22** (3):254–263.